Received: 27 November 2020 | Revised: 7 February 2021 | Accepted: 24 February 2021

DOI: 10.1002/mrm.28772

FULL PAPER

Magnetic Resonance in Medicine

Combined ^{23}Na and ^{13}C imaging at 3.0 Tesla using a single-tuned large FOV birdcage coil

Joshua D. Kaggie[1,2,3] | Titus Lanz[4] | Mary A. McLean[1,2,3] | Frank Riemer[5] | Rolf F. Schulte[6] | Arnold J. V. Benjamin[1,2,3] | Dimitri A. Kessler[1,2] | Chang Sun[1,2] | Fiona J. Gilbert[1,2,3] | Martin J. Graves[1,2,3] | Ferdia A. Gallagher[1,2,3]

[1]Department of Radiology, University of Cambridge, Cambridge, United Kingdom
[2]Cambridge University Hospitals, Addenbrooke's Hospital, Cambridge, United Kingdom
[3]Cancer Research UK Cambridge Centre, University of Cambridge, Cambridge, United Kingdom
[4]RAPID Biomedical GmbH, Rimpar, Germany
[5]Mohn Medical Imaging and Visualisation Centre (MMIV), Department of Radiology, Haukeland University Hospital, Bergen, Norway
[6]GE Healthcare, Munich, Germany

Correspondence
Joshua Kaggie, Department of Radiology, University of Cambridge, Box 218, Cambridge Biomedical Campus, CB2 0QQ, Cambridge, United Kingdom.
Email: jk636@cam.ac.uk

Purpose: An unmet need in carbon-13 (^{13}C)-MRI is a transmit system that provides uniform excitation across a large FOV and can accommodate patients of wide-ranging body habitus. Due to the small difference between the resonant frequencies, sodium-23 (^{23}Na) coil developments can inform ^{13}C coil design while being simpler to assess due to the higher naturally abundant ^{23}Na signal. Here we present a removable ^{23}Na birdcage, which also allows operation as a ^{13}C abdominal coil.
Methods: We demonstrate a quadrature-driven 4-rung ^{23}Na birdcage coil of 50 cm in length for both ^{23}Na and ^{13}C abdominal imaging. The coil transmit efficiencies and B_1^+ maps were compared to a linearly driven ^{13}C Helmholtz-based (clamshell) coil. SNR was investigated with ^{23}Na and ^{13}C data using an 8-channel ^{13}C receive array within the ^{23}Na birdcage.
Results: The ^{23}Na birdcage longitudinal FOV was > 40 cm, whereas the ^{13}C clamshell was < 32 cm. The transmit efficiency of the birdcage at the ^{23}Na frequency was 0.65 μT/sqrt(W), similar to the clamshell for ^{13}C. However, the coefficient of variation of ^{23}Na-B_1^+ was 16%, nearly half that with the ^{13}C clamshell. The 8-channel ^{13}C receive array combined with the ^{23}Na birdcage coil generated a greater than twofold increase in ^{23}Na-SNR from the central abdomen compared with the birdcage alone.
Discussion: This ^{23}Na birdcage coil has a larger FOV and improved B_1^+ uniformity when compared to the widely used clamshell coil design while also providing similar transmit efficiency. The coil has the potential to be used for both ^{23}Na and ^{13}C imaging.

Martin J. Graves and Ferdia A. Gallagher contributed equally to this study.

KEYWORDS
body imaging, carbon-13 MRI, multinuclear imaging, RF coils, sodium-23 MRI

1 | INTRODUCTION

Recent technical developments in the field of multinuclear MRI have improved spatial resolution within clinically feasible timescales, as well as allowing more accurate quantification of the measured signals. These developments have demonstrated a wide range of new clinical applications for carbon-13 (^{13}C) and sodium-23 (^{23}Na) MRI.[1-7] For example, there has been much recent interest in ^{13}C-MRI due to the advent of hyperpolarized technologies, with particular emphasis on detecting the metabolism of hyperpolarized [1-^{13}C] pyruvate into [1-^{13}C]lactate noninvasively in tumors, the heart, and in the brain.[1-3] One challenging task in the field of multinuclear MRI is ensuring optimum RF coil hardware. In this work, we focus on a transmit (Tx) RF coil for both ^{23}Na and ^{13}C excitation.

^{13}C RF coil evaluations are more challenging than those for ^{23}Na due to the low natural abundance of ^{13}C (~1%), the long T_1 values for many ^{13}C nuclei (>1.0 s for relevant molecules at 3 Tesla [T]), multiplet peaks, and the need for expensive enriched phantoms. In contrast, ^{23}Na-MRI can be performed using readily available saline phantoms in vitro; has a short T_1 (20-40 ms typical at 3.0 T[8,9]), which enables rapid TR; and is not affected by J-coupling. The high natural abundance of ^{23}Na makes it favorable for imaging in vivo. Because the RF requirements for ^{13}C-MRI and ^{23}Na-MRI are very similar due to their gyromagnetic ratios ($\gamma^{13}{}_{C}$ = 10.708 MHz/T; $\gamma^{23}{}_{Na}$ = 11.262 MHz/T), the characterization of a ^{23}Na abdominal Tx coil enables the assessment of a design prior to ^{13}C-specific coil construction.

In addition, the small difference in the 2 Larmor frequencies yields the opportunity to evaluate the feasibility of driving the ^{23}Na coil off-resonance for acquisition at the ^{13}C-frequency. Such off-resonant operation has potential benefits. We have shown that the detection of the ^{23}Na resonance, using a coil tuned to ^{13}C, can be used to calibrate the Tx B_1 and center frequency prior to hyperpolarized [1-^{13}C]pyruvate metabolism in vivo imaging. Such an approach could greatly improve the workflow for clinical ^{13}C-hyperpolarized imaging.[10] Furthermore, we have previously shown that ^{23}Na-MRI can be undertaken with an endorectal coil tuned to ^{13}C, allowing additional and complementary ^{23}Na information to be acquired during a hyperpolarized ^{13}C-MRI exam of the prostate.[11] Therefore, as part of this work we are interested in the degradation of coil performance when using a ^{23}Na coil at the nearby but off-resonant frequency of ^{13}C.

An ideal Tx coil has a high B_1^+ field uniformity and a low RF power consumption, which is particularly important for imaging large FOV regions such as the thorax or abdomen. Therefore, Tx coils typically surround the body part under investigation. An ideal abdominal Tx coil would also accommodate patients with wide-ranging body habitus, which is particularly important because many pathological conditions are associated with an increased abdominal girth due to obesity, masses, or ascites. Removable volume coils are typically required for ^{13}C or ^{23}Na imaging to avoid disruption of the clinical hydrogen-1 (^{1}H)-MRI.

However, the construction of body-sized, removable coils for multinuclear MRI is challenging because the large coil size reduces Tx efficiency. Broadband RF amplifiers used for multinuclear MRI with local RF coils are supplied with only a fraction of the available power used for ^{1}H-MRI, typically a fourth or even less. This limited available Tx power at non-^{1}H frequencies (≤8 kW for non-^{1}H vs. > 30 kW for ^{1}H at 3.0 T) necessitates an optimized Tx efficiency for effective imaging and forms the basis for the work presented here, in which ^{23}Na coil properties are assessed as a surrogate for evaluating ^{13}C RF properties more easily than a ^{13}C tuned coil. Whereas the B_1^+ field shape is largely determined by coil geometry regardless of the nucleus imaged at field strengths below ≤3.0 T, the precise assessment of SNR and Tx efficiency are due to frequency dependencies of matching and tuning.

For choosing an appropriate coil design for a ^{13}C abdominal Tx coil, we considered the coil designs common in the x-nuclei field, especially the clamshell coil[9,12-15] and various birdcage coil approaches.[16-18] The clamshell coil is a widely used, and the largest previously available, Tx-only system for ^{13}C abdominal imaging,[9,12-15] which has also been used for ^{23}Na-MRI at 1.5 T.[13,14] The clamshell consists of 2 ~30 cm Helmholtz-like loops separated by a variable distance. The 60 cm available MRI system bore diameter is further reduced by the patient table and the clamshell to 29 cm in the vertical direction and by ~45 cm in the left–right direction due to the coil support structures on one side. The requirement for separate receive (Rx) coils, which can be up to 10 cm in depth, also reduces the available volume. Furthermore, the FOV of the ^{13}C clamshell is limited by the low Tx homogeneity and the limited length in the *z* direction. This lack of available patient space has limited which patients can be imaged when using the combination of the clamshell with both anterior and posterior Rx arrays.

The aim of this study was to develop a ^{23}Na abdominal Tx coil with increased available space for patients and coverage along *z*, as compared to the commonly used clamshell coil, with improved Tx B_1^+ uniformity while maintaining Tx efficiency. ^{23}Na was used as a prototype for a ^{13}C Tx system due to the higher endogenous signals available for ^{23}Na. Whereas torso ^{23}Na birdcage coils[16-18] provide a higher B_1^+ uniformity and Tx efficiency over linear coils (due to quadrature polarization), they restrict patient space due to their closed designs, which are often built with 16 rungs. A design with significantly fewer rungs enables the imaging of patients with larger abdominal girth by allowing the patient to use the full width of the bore between the 2 end rings. Therefore, we decided to evaluate a birdcage design with only 4 rungs and asymmetric end rings to maintain the advantages of a birdcage coil design (B_1^+ homogeneity, Tx efficiency and coverage) while overcoming these space restrictions. For the evaluation of the design, we have chosen a 4 rung ^{23}Na birdcage coil. We also demonstrate the combination of ^{1}H, ^{23}Na, and ^{13}C abdominal imaging within a single setup

2 | METHODS

2.1 | ^{23}Na Tx/Rx volume coil

A custom-built Tx/Rx 4 rung, 50 cm long birdcage coil was designed (Figures 1 and 2) (Rapid Biomedical GmbH, Rimpar, Germany). The rungs were positioned 30 cm apart to resemble the loop size of the clamshell coil (loop diameter and distance ~30 cm) and consist of 50 cm long, 10 mm diameter copper tubes. The end rings were adjusted to match the MRI bore and scanner table curvature for maximizing the space for the patient. The inner part of the rungs lies on a diameter of 42 cm; the coil outer diameter is 56 cm at its maximal left-to-right dimension, matching the bore size. The conductors of the end rings are printed circuit boards with 20 mm conductor width. The coil was tuned and matched to 33.8 MHz, the ^{23}Na frequency at 3.0 T. The asymmetric shape created end-ring inductance imbalances such that the coil required additional ring capacitors (C_L in Figure 1B) to keep the electrical coil symmetry for quadrature drive. The coil includes a separate 90° hybrid splitter for quadrature drive and a low noise preamplifier with a gain of 27 dB and a 0.9 dB noise figure. Final tuning/matching of the coil was undertaken within the scanner bore.

The loaded and unloaded quality (Q) factors were measured with 2 stationary decoupled magnetic field probes inside the coil from the −3 dB bandwidth of S21 on a network analyzer. The load was a rectangular tub filled with 55 mM NaCl, approximately 32 × 22 × 22 cm^3 in dimension, containing 48 g NaCl mixed with 15 L water.

2.2 | 8 Channel Rx-only array

For testing the imaging performance, an 8 channel ^{13}C Rx-only array—4 posterior, 4 anterior (Rapid Biomedical GmbH, Rimpar, Germany)—was used inside the ^{23}Na birdcage coil. This was used for both ^{23}Na and ^{13}C signal reception without retuning any components. Although the birdcage coil could not be detuned during reception, the large differences between the Tx and Rx coil sizes resulted in low intrinsic coupling, hence obviating the need for active decoupling.

2.3 | B_1 Phantom measurements for ^{23}Na, ^{13}C, and ^{1}H

Tx efficiency and B_1^+ field uniformity was evaluated for both frequencies: ^{23}Na and ^{13}C for the ^{23}Na birdcage and ^{13}C for

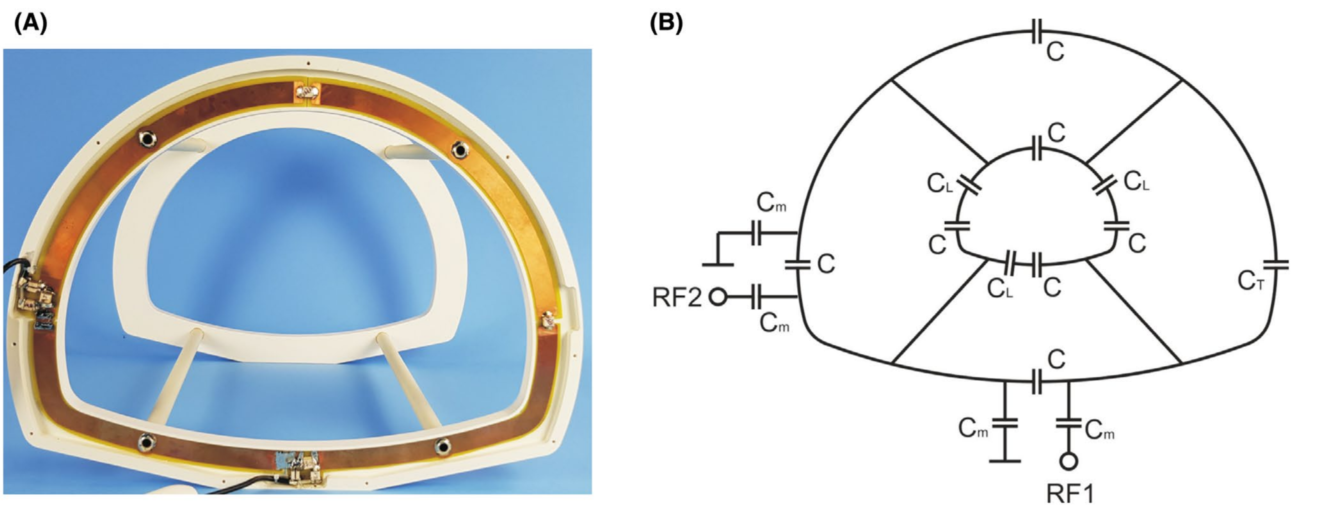

FIGURE 1 (A) Photograph of the ^{23}Na birdcage coil with the cover removed. (B) Circuit design showing the capacitors for tuning and matching, for which C is the capacitance for a symmetric birdcage tuned to 33.8 MHz and C_L has been added to achieve electrical symmetry. RF coupling occurs at the RF1 and RF2 ports. The capacitors were: C = 41 pF, C_L = 160 pF, and C_m = 38 pF for tuning/matching to 33.8 MHz inside the bore. ^{23}Na, sodium-23

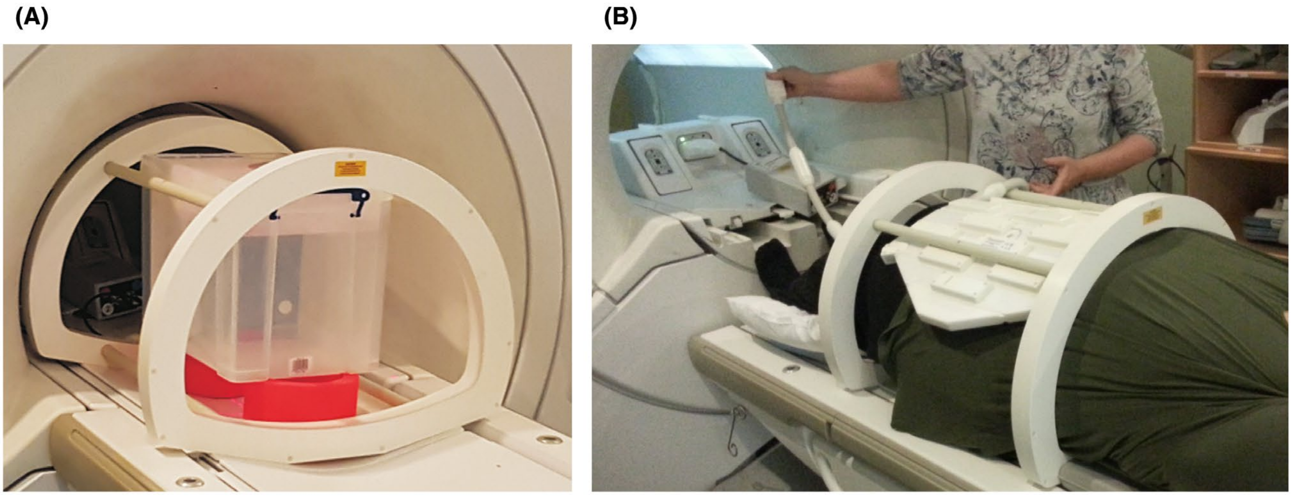

FIGURE 2 (A) The ^{23}Na 4-rung birdcage coil with saline phantom constructed for testing. (B) A female subject is shown inside the ^{23}Na birdcage, with a flexible ^{13}C receive array, demonstrating the possibility of using this system on a 118 kg volunteer. ^{13}C, carbon-13

the ^{13}C clamshell. Tx efficiency and B_1^+ maps acquired during phantom imaging were used to evaluate the safety of volunteer scanning through global-specific absorption rate (SAR) calculations and observing local RF hot spots.

^{23}Na-B_1^+ maps were obtained using the double angle mapping method with the 15 L NaCl phantom. B_1^+ maps were acquired with the birdcage coil in Tx/Rx mode at 2 flip angles (45° and 90°) using a 3D cones gradient echo (GRE) sequence: TR = 250 ms; TE = 455 μs; pulse width = 500 μs; delay 205 μs; voxel size = 6.1 × 6.1 × 6.1 mm^3; FOV = 42 cm; averages = 16; interleaves = 196; readout duration = 30 ms; scan time = 10 min 24 s; and bandwidth ±125 kHz.

The surface temperatures of the coils were measured with an infrared thermometer (PRO 8861, RS Components, UK) before and after the same 3D cones sequence but using the full available power: TR = 100 ms and flip angle = 90°, averaged for ~10 min.

^{13}C-B_1 maps were acquired using a double angle mapping in a 32 cm sphere of silicone oil (GE Healthcare, Waukesha, WI). Slices were excited with spectral-spatial pulses: nominal flip angles 60° and 120°; FOV = 48 cm; TR = 5 s; and 128 averages. ^{13}C-B_1 variation along the bore was measured by moving a 5 cm surface Rx coil along the z axis of a large rectangular phantom containing doped silicone oil; followed by maximizing the signal; and then using a 2 ms long, 90° hard pulse to measure the overall signal decrease, which was considered to be the relative B_1^+ change.

In order to ensure safety during ^{1}H imaging using the MRI system body coil, the interactions with the ^{23}Na removable birdcage coil were assessed by ^{1}H-B_1^+ field measurements on 2 adjacent rectangular (32 × 22 × 18 cm^3) phantoms containing dimethyl silicone fluid, gadolinium, and pink colorant[19] (GE 283, GE Healthcare). The phantoms were placed close to the rungs to replicate maximum local ^{1}H-B_1^+ distortion. The 2D ^{1}H-B_1^+ maps were acquired using a Bloch-Siegert method with a spoiled GRE sequence: TR = 29 ms; TE = 13.2 ms; flip angle = 20°; 3.75 × 3.75 mm^2; FOV = 48 cm; 20 slices with 10 mm thickness; and ±16 kHz bandwidth. To further improve safety during human imaging, the pulse widths were doubled compared to typical ^{1}H sequences, which reduces SAR by a factor of 2. After phantom validation, the Tx flip angle was slowly increased during the initial in vivo experiments while ensuring that the subject did not experience any excess heat.

2.4 | Calibration measurements

Bloch-Siegert calibration scans were performed on 6 normal volunteers (5 male/1 female; ages = 38 ± 13 years; body mass index [BMI] = 25 ± 3 kg/m^2) to obtain the center frequency and the power required for a nominal 90° pulse. The forward transmission (S21) was also measured between the 0° and 90° coil ports to evaluate quadrature stability. The Tx gain is reported in centibels (cB), whereas RF measurements are reported in decibels (dB) as per vendor and community naming conventions, respectively.

2.5 | Normal volunteer imaging

After safety was assured, imaging was performed on a single, normal volunteer (male, [body mass index] = 28 kg/m^2) using a 3T MRI system (MR750, GE Healthcare) and following written informed consent and ethical approval (Hertfordshire Research Ethics Committee REC ref 08/H0311/117, IRAS 161555). Before imaging at the ^{13}C or ^{23}Na frequency, the default eddy current correction values were modified for the nucleus of interest.[20] Matched 2D GRE single-shot spiral images were obtained using a nominal 60 × 60 point readout for ^{13}C and ^{23}Na: TR = 250 ms (^{13}C) and 150 ms

(^{23}Na); TE = 12 ms and 0.70 ms; flip angle =70°; voxel size = 8 × 8 × 80 mm^3 (^{13}C) and 8 × 8 × 40 mm^3 (^{23}Na); FOV = 48 cm; averages = 128; and bandwidth = ±125 kHz. The ^{13}C data were acquired with spectral–spatial excitation at the frequency of a natural abundance fat peak.

Fat and water were imaged with the ^{1}H body coil using a 3D in- and out-of-phase spoiled GRE: TR = 4.0 ms; TE = 1.1 ms (in)/2.2 ms (out); flip angle = 15°; matrix size = 256 × 192 × 120; voxel size = 1.9 × 1.9 × 5.0 mm^3; and partial phase sampling of 70%. To limit the possibility of excess patient heating during ^{1}H imaging, only a single GRE sequence was scanned, and only after the results of phantom experiments.

3D cones ^{23}Na GRE images were acquired: TR = 100 ms; TE = 705 µs; pulse width = 1.0 ms; delay = 205 µs; flip angle = 70°; voxel size = 4 × 4 × 8 mm^3; FOV = 48 cm; 1402 interleaves; readout duration = 30 ms; and bandwidth = ±83 kHz. The number of averages was 5 with the phased array, and 4 with the body coil only, resulting in total scan time of 11 min 42 s and 9 min 21 s, respectively. This difference in averages results in an 11% ($= \sqrt{\frac{5}{4}}$) SNR increase.

3 | RESULTS

3.1 | Bench measurements

The S11 of the loaded coil at either ^{23}Na birdcage port (0° and 90°) was −34 dB, and S21 between the 2 ports was −25 dB at ^{23}Na frequency. The S11 was −16 dB at the ^{13}C frequency. The unloaded Q factor was ~800 and decreased to ~25 when loaded with the 15 L NaCl phantom. Coupling with the MRI system caused a ~2.6 MHz frequency shift.

Active decoupling (ΔS21 acquired with dual pickup loop) of any Rx loop of the ^{13}C array was better than 30 dB (active coil −36 dB vs. deactivated coil −75 dB) at ^{13}C frequency when measured with 2 external decoupled magnetic probes. At the ^{23}Na frequency, each of the ^{13}C array loops showed a ΔS21 of ~16 dB (−44 dB to –60 dB). Preamplifier decoupling was 14 dB (−38 dB to −52 dB) for ^{13}C and 4 dB (−47 dB to −51 dB) for ^{23}Na.

3.2 | Tx properties

The Tx efficiency of the ^{23}Na birdcage at the ^{23}Na frequency was 0.65 µT/sqrt(W) and for the ^{13}C clamshell coil at the ^{13}C frequency was 0.63 µT/sqrt(W). The power consumption of the ^{23}Na birdcage was increased by a factor of 2 when being driven off-resonant at the ^{13}C frequency, resulting in a decrease of Tx efficiency by a factor of 1.4.

Figure 3 shows ^{23}Na flip angle ($\propto B_1^+$) maps in 3 directions, with the phantom positioned as shown in Figure 2A. The mean flip angle was 90° ± 16°, or coefficient of variation = 18%, as measured throughout the entire central axial slice of the phantom for the ^{23}Na birdcage. Within the same phantom slice, 30% of the ^{23}Na birdcage voxels had a B_1 between 100 and 120% of the mean, and 60% between 80 and 100%.[10]

A central axial map (Figure 3A) demonstrates nonuniformity at the periphery of the ^{23}Na birdcage FOV with up to a 50% increase in ^{23}Na-B_1^+ in 2 regions near the coil rungs, although this is not observed in either central sagittal or coronal images.

Figure 4A,B show ^{13}C-B_1^+ maps acquired with the clamshell coil. The coefficient of variation was 28% over the central slice, and 18% of its voxels were between 100 and 120% of the mean B_1^+. Thirty percent of its voxels were within 80% and 100% of its mean B_1^+.

Figure 5 compares the B_1^+ falloff in the craniocaudal direction of both the ^{23}Na birdcage for ^{23}Na using the 32 cm long saline phantom, and ^{13}C clamshell for ^{13}C using a 5 cm loop adjusted in its longitudinal position along a silicone oil phantom. The ^{23}Na birdcage has lost less than 10% of its maximum B_1^+ at 16 cm at the edge of the phantom, for which the ^{13}C clamshell was 35% below its maximum.

The regions of interest of the ^{1}H-B_1^+ maps are shown in Figure 6 with the phantoms immediately above the rungs. The relative mean ^{1}H-B_1^+ using the standard body coil of 100 ± 11% when the ^{23}Na birdcage was in the bore increased to 192% ± 2% when the ^{23}Na birdcage was removed when measured without additional Tx power readjustment. After recalibration using automatic prescan adjustment, the body coil had a relative mean ^{1}H-B_1^+ of 100% ± 2%. When the ^{23}Na birdcage was in place, the relative ^{1}H-B_1^+ decreased by 50% near the birdcage rungs, whereas just outside birdcage the ^{1}H-B_1^+ was nearly twice the nominal value.

No portion of the ^{23}Na birdcage had a temperature change of more than 1°C after sodium phantom studies.

3.3 | Noise correlation

Figure 7 shows the noise correlation between all the Rx elements of the ^{13}C array, measured at both frequencies with the subject in place. The noise correlations were < 10% between any 2 coils at either frequency. The correlations were not a constant ratio between the 2 frequencies, which suggests that the coil elements have mild frequency-dependent responses, which can similarly be observed by the lower off-resonant preamplifier decoupling.

3.4 | Calibration measurements

The calibration scans on normal volunteers demonstrated the following results: center frequency = 33,799,288 ± 7 Hz; Tx gain = 186 ± 10 cB; and |S21| was 12.4 ± 0.9 dB (mean ±

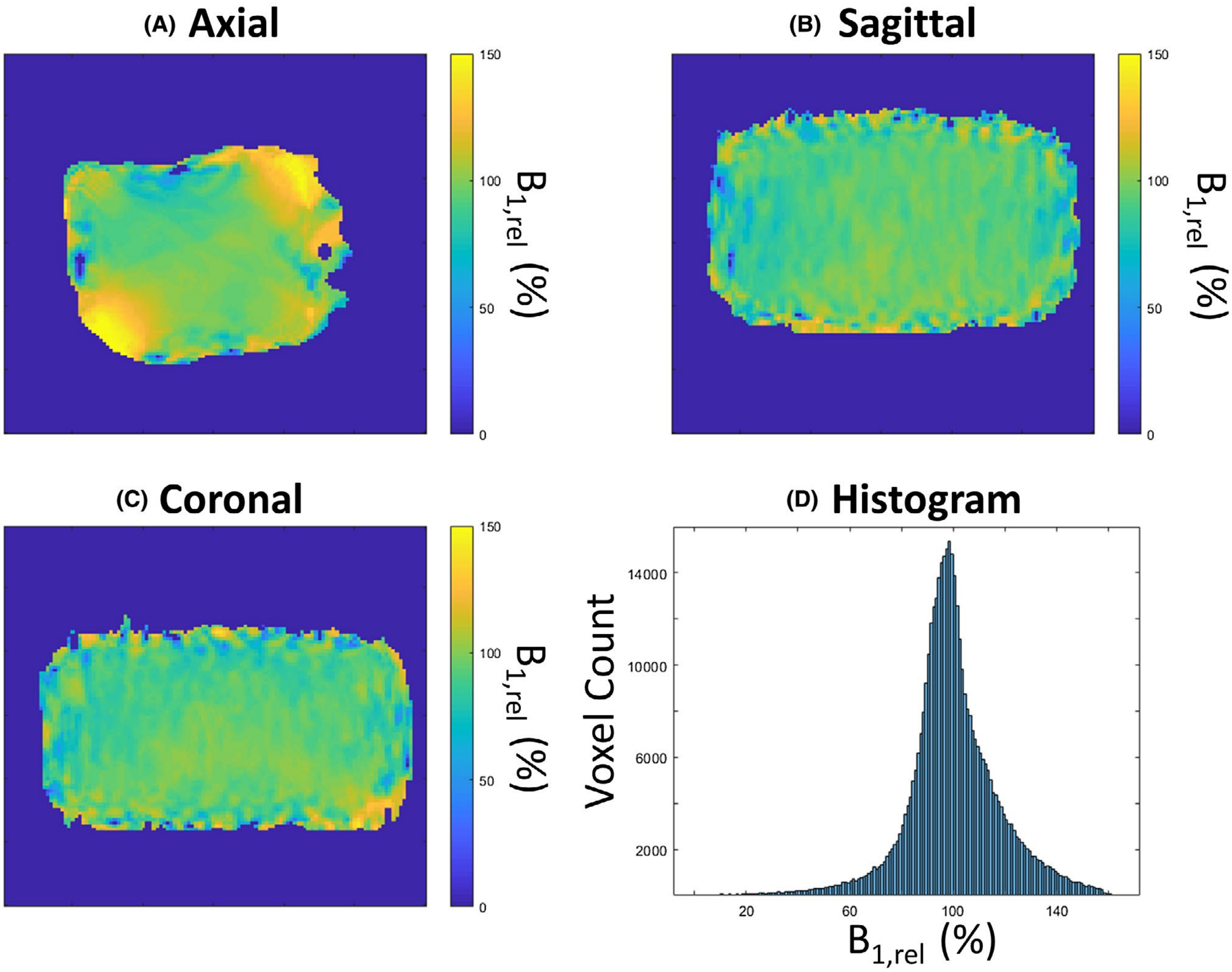

FIGURE 3 (A-C) ^{23}Na-B_1 maps of the 15 L NaCl phantom along each orthogonal direction acquired using dual angle mapping and a saline phantom. (D) Histogram of the flip angles throughout the phantom.

SD). There were no linear correlations between any combination of body mass index, center frequency, or Tx power (P values > .25).

3.5 | Imaging

The small number of rungs enabled the possibility of imaging a large volunteer (Figure 2B). The limitation on patient size with this coil setup is primarily determined by the scanner bore width, unless the hips or shoulders are placed near the end ring; however, the length of the coil and the large z coverage minimize the requirement for this.

Figures 8 and 9 show in vivo ^{23}Na MRI of the kidneys, liver, spleen, spine, and aorta. Figure 8 shows imaging of both the natural abundance ^{13}C signal from fat and endogenous ^{23}Na using the ^{13}C array (Rx) with the ^{23}Na birdcage (Tx). The 50 cm length of the coil allows ^{23}Na imaging from the level of the heart to the pelvis, while obtaining a 90° flip angle with a 1 ms rectangular pulse width using an 8 kW power amplifier. The Tx gain was 188 cB, which for a maximum Tx gain of 200 cB translates to a power used that was within 15% below the maximum. If the ^{23}Na birdcage were tuned to ^{13}C, we expect to have a similar power requirement.

4 | DISCUSSION

We have demonstrated the feasibility of using a ^{23}Na birdcage coil for large FOV ^{23}Na and ^{13}C imaging within the abdomen. Our Tx coil is larger than any commercially available coils previously reported for ^{13}C imaging. The insertable ^{23}Na birdcage enables a craniocaudal FOV up to 48 cm, which is comparable to both conventional ^{1}H imaging and to previously reported ^{23}Na systems.[16]

The unloaded-to-loaded Q ratio, measured on the ^{23}Na birdcage, is very high (> 30), as occurs with large coils due to an increase of sample losses and resistance.[21] The drop in Q when loading the coil demonstrates that the setup is sample noise dominated, and a gain in Tx efficiency can only

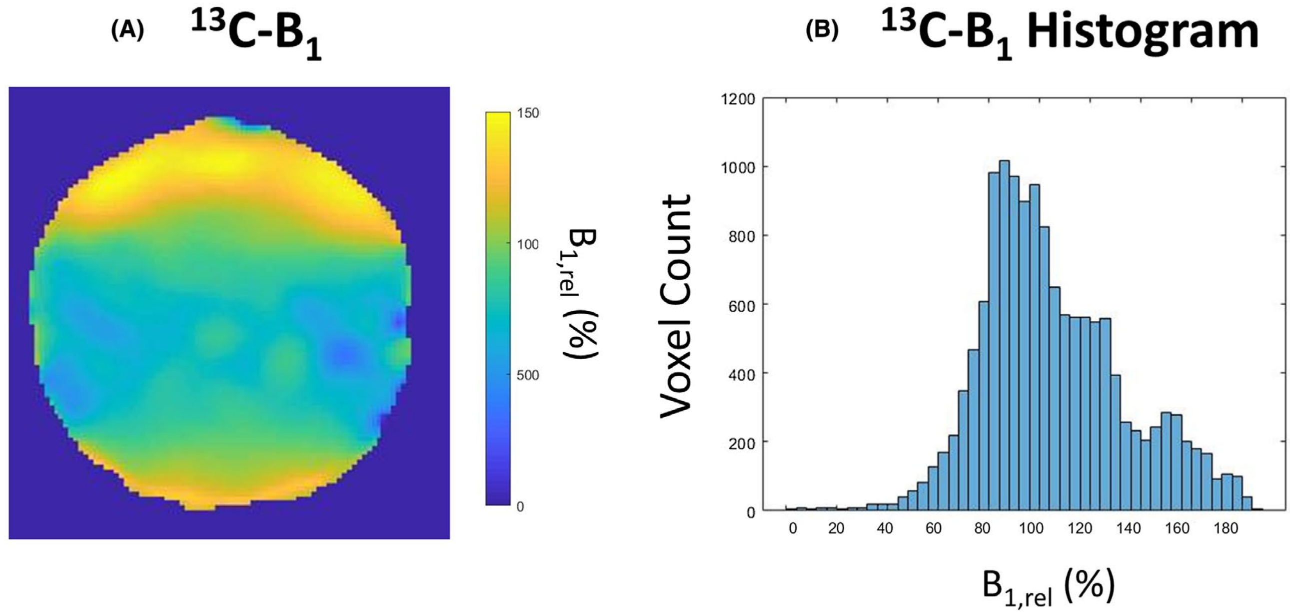

FIGURE 4 Axial clamshell ^{13}C-B1 map (A) and corresponding histogram (B) using a 32 cm silicone sphere phantom. The clamshell has a B_1 distribution that is broader than the ^{23}Na distribution and is multi-modal.

FIGURE 5 The relative B_1 along the *z* axis from the center of the phantom for both the ^{23}Na birdcage at ^{23}Na frequency and the ^{13}C clamshell at ^{13}C frequency, demonstrating greater consistency for the birdcage.

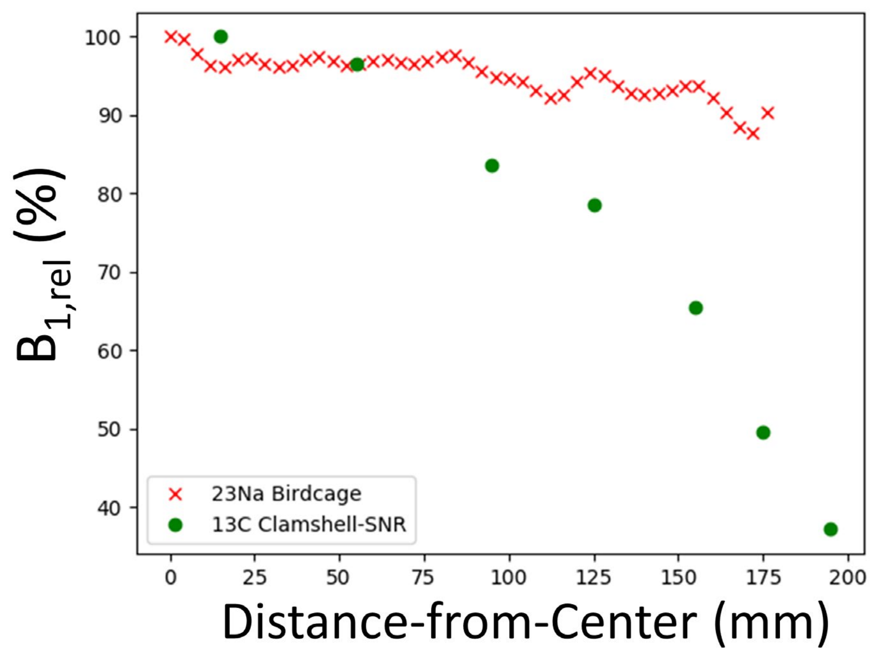

be achieved by changing the *z* coverage of the coil. The Tx efficiencies of both birdcage and clamshell coils are similar at their optimized frequencies. Both coils have a similar cross-section in the axial plane, with the birdcage being ~67% longer. The expected drop of 23% in Tx efficiency due to additional length is compensated by the gain in quadrature (40%). Therefore, a 90˚ flip angle was achievable with a hard pulse width of 1.0 ms and < 8 kW power, which is often difficult to achieve with a large linear clamshell coil due to the higher nonuniformity and SAR. Whereas shorter pulse durations are desirable for ^{23}Na imaging, a 1.0-ms pulse is a simple number that is useful for comparisons, especially considering the RF amplifier power limitations. The pulse duration could not be shortened by more than 0.2 ms (eg, below 0.8 ms) due to insufficient Tx to achieve the desired flip angles.

The Tx efficiency demonstrated here was favorable compared to the reported Tx efficiency of a ^{23}Na abdominal birdcage reported by Wetterling et al. (0.5 ms block pulse, 90°, 1200 V, 0.24 μT/sqrt(W)[17]). The lower Tx efficiency of

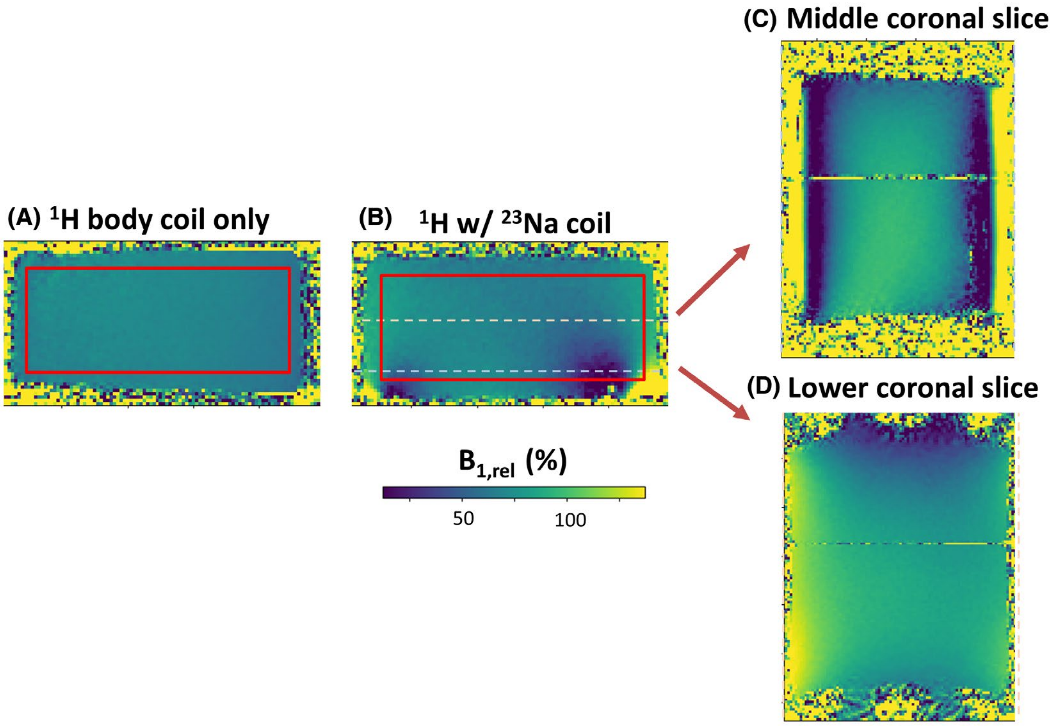

FIGURE 6 Axial proton B_1 maps of 2 large 12.7 L phantoms acquired using the standard ^{1}H body coil: (A) without the ^{23}Na coil inside the system and (B-D) with the ^{23}Na coil inside the system. (A) Demonstration of a uniform B_1 field without the insert. (B-D) Demonstration of ^{1}H shielding immediately near the ^{23}Na-coil rungs. Images (C) and (D) show 2 parallel coronal slices, with a split occurring between the phantoms. The red boxes in (A) and (B) indicate the regions of interest used for calculation. The dashed lines in (B) indicate the 2 orthogonal slices shown in (C) and (D). ^{1}H, hydrogen-1

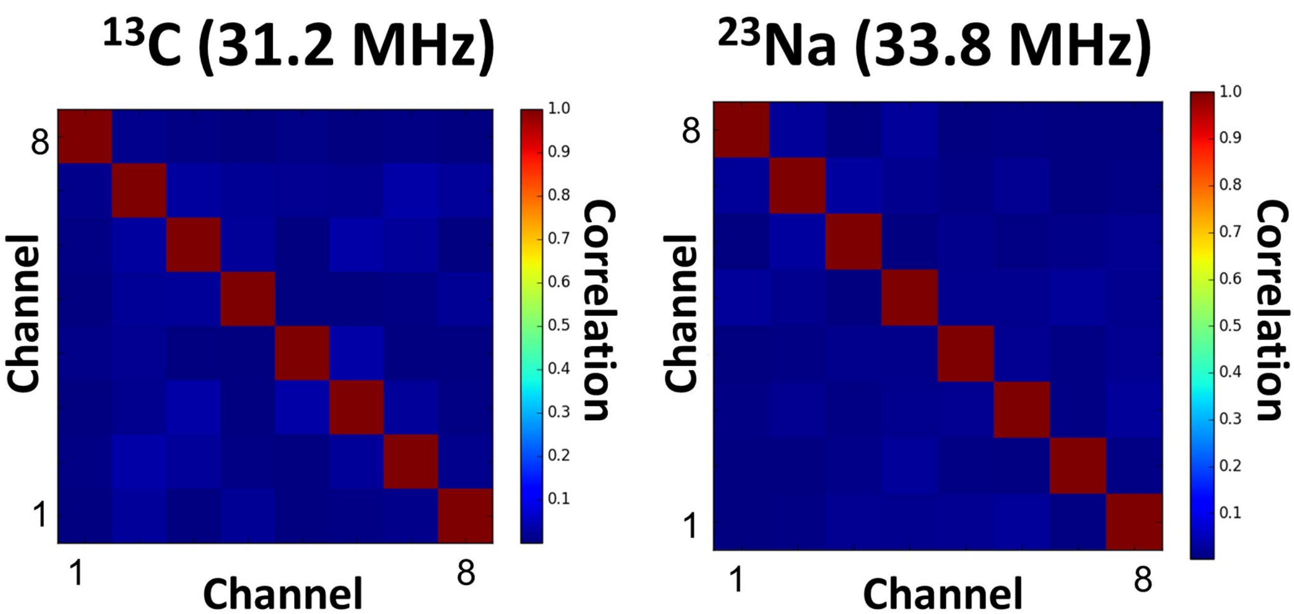

FIGURE 7 Noise correlation matrices of the 8channel ^{13}C array, measured at 32.1 MHz for ^{13}C and at 33.8 MHz for ^{23}Na. The noise correlation between any 2 coils was < 10% at either frequency, suggesting the coils are decoupled.

Wetterling et al. is mainly due to the routing of RF power for ^{23}Na and suboptimal quadrature performance due to the elliptical shape of their birdcage coil (personal communication with the authors). The Tx efficiency of our ^{23}Na birdcage at the off-resonant ^{13}C frequency decreased by 30% but still allowed acceptable ^{13}C imaging. Because the decreased Tx

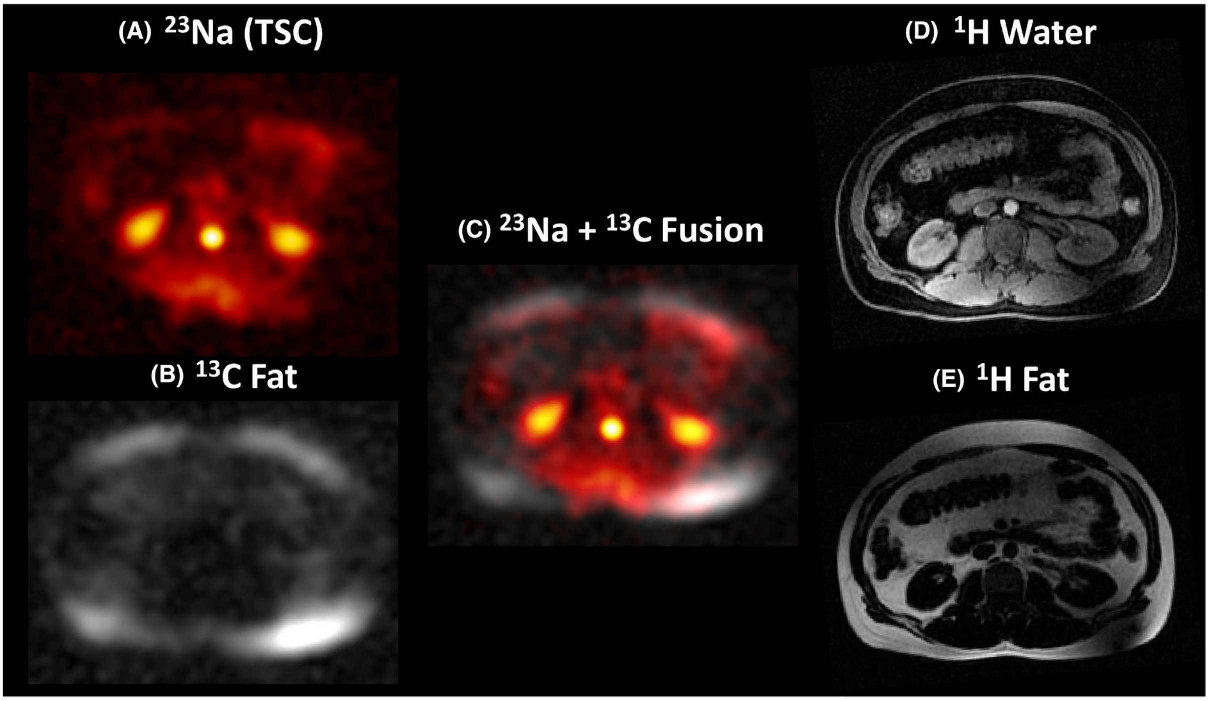

FIGURE 8 Axial images of the abdomen showing: (A) sodium images, and (B) natural abundance ^{13}C from fat using the same spiral GRE pulse sequence with the ^{23}Na birdcage coil as the transmit coil and the ^{13}C 8 channel array as the receive coil with the volunteer in the same position. (C) A fusion image showing ^{23}Na signal overlaid onto the ^{13}C fat images, which is used here to evaluate both nuclei. Corresponding (D) water and (E) fat images acquired with the ^{1}H body coil and the ^{23}Na birdcage in place using in- and out-of-phase fat/water imaging. GRE, gradient echo

efficiency does not influence the SNR of an additional ^{13}C Rx coil (as long as the required flip angles can be achieved), such a single tuned coil is capable of exciting both ^{23}Na and ^{13}C in a single setup as part of a multinuclear scan.

The ^{23}Na birdcage also enables higher uniformity, showing half the B_1^+ coefficient of variation and a more symmetrical distribution on a histogram of B_1^+ values. The circular polarization of the ^{23}Na birdcage improves field uniformity by adding an orthogonal field pattern that is complementary to a linearly driven coil and compensates for design intrinsic B_1^+ field nonuniformities due to imperfect tuning. The ^{13}C-B_1 maps of the ^{13}C clamshell coil show an hourglass-shaped field pattern. Even with only 4 rungs, the periphery of the ^{23}Na-FOV does not demonstrate severe B_1^+ changes (< 50% increases). B_1^+ uniformity simplifies quantitative imaging, improves safety assessments, and can improve SNR when combined with Rx-only coils.

The bore diameter is a limiting factor when accommodating large patients within an MRI system. However, diameter alone is not the only geometric factor that determines patient comfort within a coil: the 4 rung birdcage that we demonstrate here is less restrictive than a clamshell coil design or a 16 rung birdcage (see Figure 2), enabling larger patients to be imaged and more comfortably positioned. Future iterations of this coil will incorporate a split design for easier patient positioning.[22,23] The increase in z length from 30 cm to 50 cm provides the coverage required for whole abdominal imaging that is not possible with the clamshell design, which is in widespread use.

Because the ^{23}Na birdcage is present in the bore during transmission of both ^{23}Na and ^{1}H, the safety of the coil with regard to RF deposition for all frequencies must be considered. The reduction of ^{1}H-B_1^+ field of the integrated ^{1}H body coil when the ^{23}Na birdcage is placed inside the bore shows that the ^{23}Na birdcage has an RF shielding effect. The shielding results in a twofold lower B_1^+ field amplitude and therefore E-field at this frequency. Substantial ^{1}H-B_1^+ field inhomogeneities were not observed close to the rungs or rings internal to the ^{23}Na birdcage, which might have been a sign for local SAR hot spots. The ^{1}H-$B_1^+B_1$ was increased by 50% immediately external to the coil near its rungs such that increased ^{1}H-SAR must be considered at this point for ensuring patient safety. We restricted our ^{1}H sequences to a GRE sequence to improve safety, which has over sixfold lower SAR than conventional steady-state fast spin echo sequences.

^{23}Na sequences are SNR-efficient at very short TRs and high flip angles and therefore need consideration of SAR. Because the ^{23}Na birdcage is a volume coil, whole body SAR and partial body SAR restrictions must be adhered to within the abdomen in order to confine the heating of patient tissue to an acceptable limit according to International Electrical Commission standards (60601-2-33[24]). The low frequency

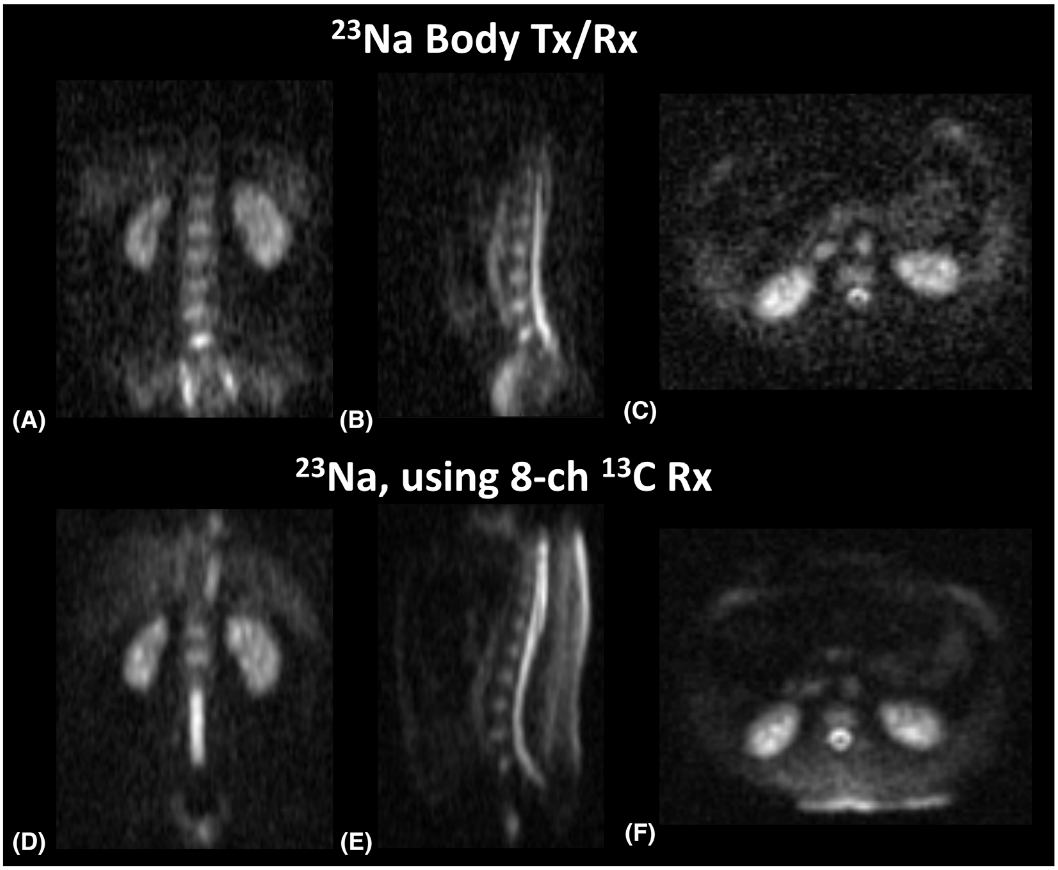

FIGURE 9 4 × 4 × 8 mm^3 3D cones imaging reformatted into: (A, D) coronal, (B, E) sagittal, and (C, F) axial ^{23}Na images of a normal volunteer. (A-C) Acquired using only the ^{23}Na body coil for transmit and receive, and (D-F) using the ^{23}Na body coil for transmit in conjunction with a ^{13}C 8 channel array for ^{23}Na receive. The 8channel array results in approximately twice the SNR in the kidneys, which allows easier differentiation of cortical and medullary regions.

TABLE 1 SNRs (mean ± SD) for ^{23}Na signal in several abdominal regions in 1 volunteer, using the ^{23}Na birdcage only, and using the 8-channel ^{13}C array in conjunction with the ^{23}Na birdcage

Region	^{23}Na-SNR (^{23}Na Birdcage Tx/Rx)	^{23}Na-SNR (^{13}C 8 channel Rx)	Number of Voxels
Right kidney	10.5 ± 1.5	18.0 ± 2.4	2153
Left kidney	9.5 ± 1.5	18.6 ± 2.6	2226
Liver	2.8 ± 1.1	6.0 ± 1.4	4519
Aorta	13.3 ± 2.9	27.5 ± 5.0	1251
Skin	<1.7	20.2 ± 6.7	1339

The values shown using the birdcage have been increased by 11% to correct for differences in the number of averages.

of the ^{23}Na birdcage enables the use of B_1^+ maps as a proxy for simulations to estimate SAR. The ^{23}Na-B_1^+ field increases near the rungs were sufficiently low for safe ^{23}Na operation under standard limits. Theoretically, when using a similar B_1^+ pulse width and shape, a birdcage can have more than twofold less SAR centrally than a linear coil (eg, the clamshell) due to quadrature operation.[24]

For safe operation of the ^{23}Na birdcage as a Tx coil for the ^{13}C Rx array, this array needs to be appropriately decoupled at each working frequency. For achieving sufficient decoupling at the ^{13}C frequency, the ^{13}C array incorporates actively switched ^{13}C traps. Although decoupling traps are narrow band components, our tests showed that the ΔS12 of the ^{13}C array at the ^{23}Na frequency is still sufficient to protect the array electronics from excessive ^{23}Na-RF. In addition, phantom imaging did not show additional local ^{23}Na-B_1^+ hot spots. Therefore, the ^{13}C decoupling was sufficient for component protection and patient safety during both ^{13}C and ^{23}Na-MRI. There are confounding factors when Rx coils are used off-resonance: the decoupling strength will be lower for off-resonant traps, but a nonresonant coil will also receive lower levels of power such that the decoupling does not require the same strength.

The difference between the large resonator size of the Tx coil as compared to the smaller Rx coil elements results in a low inductive coupling; and given that the Tx coil was not detuned during Rx, the SNR is not reduced. The ^{13}C array coil showed 2 to 3 times the ^{23}Na-SNR within the abdomen centrally compared to the ^{23}Na birdcage in Tx/Rx mode, with even higher SNR ratios closer to the array. Qualitative results show comparable ^{23}Na image quality in the kidneys when our array is compared with a 7.0T 4 channel setup.[25] The preamplifier decoupling at ^{23}Na frequency was suboptimal due to the fact that a ^{13}C Rx array was used for these experiments, although the distance between loops and geometric decoupling reduced some of the correlated noise. Our results are similar to previously published ^{23}Na results using a volume and Rx coil setup[16] for which ~3 times the SNR was achieved with a ^{23}Na array compared to a ^{23}Na volume coil.

The B_1^+ field patterns at ^{13}C can be assumed to be the similar as for ^{23}Na-Tx.[26] The loaded Q factor of ~25 results in a bandwidth of 1.2 to 1.4 MHz (BW = f_0/Q), enabling the ^{23}Na coil to cover ^{13}C with 50% insertion loss, which was still sufficient for ^{13}C imaging. However, for optimum performance at ^{13}C, a dedicated ^{13}C birdcage is preferable. The ^{13}C-SNR was maintained by the dedicated ^{13}C Rx array, which performed sufficiently well to obtain a natural abundance ^{13}C fat image, despite its potential for electromagnetic coupling to the ^{23}Na birdcage that was not detuned during Rx.

Utilizing all the capabilities of this design, we showed that combined imaging of ^{23}Na, ^{13}C, and ^{1}H was possible in this setup, as demonstrated in Figure 8. For ^{1}H, the built-in body coil was used, whereas for ^{23}Na and ^{13}C imaging the ^{23}Na birdcage was used for Tx and the ^{13}C array was used for Rx. We have previously demonstrated the converse approach in the prostate with a ^{23}Na Rx and ^{13}C clamshell Tx.[11] This approach of merging ^{23}Na and ^{13}C imaging into a single-tuned coil setup that is capable of dual frequency operation is very promising for future applications of combined ^{23}Na and ^{13}C imaging without additional hardware costs.

Body coils been shown for other nuclei, such as ^{129}Xe and ^{31}P.[22,23] ^{129}Xe imaging of the lungs follows inhalation of hyperpolarized ^{129}Xe, which has a gyromagnetic ratio magnitude that is 5% higher than ^{23}Na.[22,23,27] Integrated body coils have been shown for single-tuned ^{31}P imaging at 7.0T.[27] An internal, integrated dual-tuned coil approach may gain several centimeters in diameter but would have reduced craniocaudal coverage compared to our approach. The removable approach also does not require additional regulatory approval for conventional ^{1}H imaging to prevent disruption of the integrity of existing imaging.

5 | CONCLUSION

We have demonstrated a 50 cm long, 4 rung ^{23}Na birdcage coil with asymmetric end rings with good Tx efficiency and very high field uniformity that is also suitable for ^{13}C imaging. The large craniocaudal FOV of this ^{23}Na birdcage allows coverage comparable to conventional ^{1}H imaging. When used in conjunction with an 8 channel ^{13}C Rx coil, we demonstrated a twofold increase in ^{23}Na-SNR as measured in the central abdomen, despite the ^{13}C array not being tuned to ^{23}Na. The ^{23}Na birdcage design will be transferred to a coil optimized for ^{13}C in the future and will incorporate patient access by detachable housing to enable large FOV abdominal imaging for hyperpolarized ^{13}C-MRI.

ACKNOWLEDGEMENT

Supported by funding from Cancer Research UK (CRUK) grants C19212/A16628, C19212/A27150); the European Union's Horizon 2020 Research and Innovation Programme, Grant Agreement 76121; the National Institute of Health Research (NIHR) Cambridge Biomedical Research Centre (BRC-1215-20014); Addenbrooke's Charitable Trust; the CRUK Cambridge Centre grants (C9685/A25177); GlaxoSmithKline; the CRUK & Engineering and Physical Science Research Council (EPSRC) Cancer Imaging Centre in Cambridge and Manchester grants C197/A16465; the Mark Foundation for Cancer Research; The Evelyn Trust; CRUK National Cancer Imaging Translational Accelerator (NCITA) grants (C42780/A27066); and Cambridge University Hospitals NHS Foundation Trust. The views expressed are those of the author(s) and not necessarily those of the funders.

CONFLICT OF INTEREST

Titus Lanz works for Rapid Biomedical. Dimitri Kessler receives funding from GlaxoSmithKline.

ORCID

Joshua D. Kaggie https://orcid.org/0000-0001-6706-3442
Mary A. McLean https://orcid.org/0000-0002-3752-0179
Frank Riemer https://orcid.org/0000-0002-3805-5221
Arnold J. V. Benjamin https://orcid.org/0000-0003-2063-8258
Martin J. Graves https://orcid.org/0000-0003-4327-3052

REFERENCES

1. Granlund KL, Tee S-S, Vargas HA, et al. Hyperpolarized MRI of human prostate cancer reveals increased lactate with tumor grade driven by monocarboxylate transporter 1. *Cell Metab*. 2020;31:105-114.e103.
2. Lee CY, Soliman H, Geraghty BJ, et al. Lactate topography of the human brain using hyperpolarized 13C-MRI. *Neuroimage*. 2020;204:116202.
3. Rider OJ, Apps A, Miller JJ, et al. Noninvasive in vivo assessment of cardiac metabolism in the healthy and diabetic human heart using hyperpolarized 13C MRI. *Circ Res*. 2020;126:725-736.
4. Wang ZJ, Ohliger MA, Larson PE, et al. Hyperpolarized 13C MRI: state of the art and future directions. *Radiology*. 2019;291:273-284.
5. Thulborn KR. Quantitative sodium MR imaging: a review of its evolving role in medicine. *Neuroimage*. 2018;168:250-268.

6. Bangerter NK, Kaggie JD, Taylor MD, Hadley JR. Sodium MRI radiofrequency coils for body imaging. *NMR Biomed*. 2016;29:107-118.
7. Madelin G, Lee J-S, Regatte RR, Jerschow A. Sodium MRI: methods and applications. *Prog Nucl Magn Reson Spectrosc*. 2014;79:14-47.
8. Gomolka RS, Ciritsis A, Meier A, Rossi C. Quantification of sodium T1 in abdominal tissues at 3 T. *MAGMA*. 2020;33:439-446.
9. Zöllner FG, Konstandin S, Lommen J, et al. Quantitative sodium MRI of kidney. *NMR Biomed*. 2016;29:197-205.
10. Collins CM, Li S, Smith MB. SAR and B1 field distributions in a heterogeneous human head model within a birdcage coil. *Magn Reson Med*. 1998;40:847-856.
11. Barrett T, Riemer F, McLean MA, et al. Molecular imaging of the prostate: comparing total sodium concentration quantification in prostate cancer and normal tissue using dedicated 13C and 23Na endorectal coils. *J Magn Reson Imaging*. 2020;51:90-97.
12. Nelson SJ, Kurhanewicz J, Vigneron DB, et al. Metabolic imaging of patients with prostate cancer using hyperpolarized [1-13C] pyruvate. *Sci Transl Med*. 2013;5:198ra108.
13. Steidle G, Graf H, Schick F. Sodium 3-D MRI of the human torso using a volume coil. *Magn Reson Imaging*. 2004;22:171-180.
14. Barrett T, Riemer F, McLean MA, et al. Quantification of total and intracellular sodium concentration in primary prostate cancer and adjacent normal prostate tissue with magnetic resonance imaging. *Invest Radiol*. 2018;53:450-456.
15. Tropp J, Lupo JM, Chen A, et al. Multi-channel metabolic imaging, with SENSE reconstruction, of hyperpolarized [1-13C] pyruvate in a live rat at 3.0 tesla on a clinical MR scanner. *J Magn Reson*. 2011;208:171-177.
16. Malzacher M, Chacon-Caldera J, Paschke N, Schad LR. Feasibility study of a double resonant (1H/23Na) abdominal RF setup at 3 T. *Zeitschrift für Medizinische Physik*. 2019;29:359-367.
17. Wetterling F, Corteville DM, Kalayciyan R, et al. Whole body sodium MRI at 3T using an asymmetric birdcage resonator and short echo time sequence: first images of a male volunteer. *Phys Med Biol*. 2012;57:4555-4567.
18. Platt T, Umathum R, Fiedler TM, et al. In vivo self-gated 23Na MRI at 7 T using an oval-shaped body resonator. *Magn Reson Med*. 2018;80:1005-1019.
19. Skloss T. Phantom fluids for high field MR imaging. In Proceedings of the 12th Annual Meeting of ISMRM, Kyoto, Japan, 2004. p. 1635.
20. McLean MA, Hinks RS, Kaggie JD, et al. Characterization and correction of center-frequency effects in X-nuclear eddy current compensations on a clinical MR system. *Magn Reson Med*. 2021;85:2370-2376.
21. Gruber B, Froeling M, Leiner T, Klomp DW. RF coils: a practical guide for nonphysicists. *J Magn Reson Imaging*. 2018;48:590-604.
22. Dregely I, Ruset IC, Wiggins G, et al. 32-channel phased-array receive with asymmetric birdcage transmit coil for hyperpolarized xenon-129 lung imaging. *Magn Reson Med*. 2013;70:576-583.
23. De Zanche N, Chhina N, Teh K, Randell C, Pruessmann KP, Wild JM. Asymmetric quadrature split birdcage coil for hyperpolarized 3He lung MRI at 1.5T. *Magn Reson Med*. 2008;60:431-438.
24. Jin J, Chen J. On the SAR and field inhomogeneity of birdcage coils loaded with the human head. *Magn Reson Med*. 1997;38:953-963.
25. Boehmert L, Kuehne A, Waiczies H, et al. Cardiorenal sodium MRI at 7.0 Tesla using a 4/4 channel 1H/23Na radiofrequency antenna array. *Magn Reson Med*. 2019;82:2343-2356.
26. Grist JT, Hansen ESS, Sánchez-Heredia JD, et al. Creating a clinical platform for carbon-13 studies using the sodium-23 and proton resonances. *Magn Reson Med*. 2020;84:1817-1827.
27. van Houtum Q, Welting D, Gosselink W, Klomp DW. Arteaga de Castro C, van der Kemp W. Low SAR 31P (multi-echo) spectroscopic imaging using an integrated whole-body transmit coil at 7T. *NMR Biomed*. 2019;32:e4178.

How to cite this article: Kaggie J, Lanz T, McLean MA, et al. Combined ^{23}Na and ^{13}C imaging at 3.0 Tesla using a single-tuned large FOV birdcage coil. *Magn Reson Med*. 2021;00:1–12. https://doi.org/10.1002/mrm.28772